UNIVERSITY OF TARTU
INSTITUTE OF ECOLOGY AND EARTH SCIENCES
DEPARTMENT OF GEOLOGY

Marian Külaviir

# Geopolymerization of the Estonian oil shale solid heat carrier retorting waste ash: characterization of structural changes through infrared (ATR-FTIR) and nuclear magnetic resonance spectroscopic ($^{29}$Si MAS-NMR) analysis

BSc thesis

Supervisors: Päärn Paiste
Martin Liira

TARTU 2014

# TABLE OF CONTENTS

# 1. INTRODUCTION

New inorganic materials called geopolymers which could potentially replace conventional cements, plastics and many mineral based products are becoming important in the reduction of world pollution. Pollutants, resulting from the manufacturing and use of the older materials, including large $CO_2$ emissions from producing the Portlanc cement, toxic metal contamination of freshwater resources resulting from mining operations and fires involving ordinary organic plastics. Producing cement from geopolymers instead of Portland cement would be 60% energy-efficient and emit up to 80% less carbon dioxide (Li *et al.* 2012).

For synthesising geopolymers aluminosilicate raw material is needed. In Estonia just such sources are available: oil shale ash from energy and shale-oil industry. It is possible to produce geopolymeric construction materials of these residues enabling to make use of industrial by-products and also reduce $CO_2$ footprint and energy consumption. In addition the geopolymeric building materials would diversify the local market and possibly being potential export article.

Use of oil shale for fuel in thermal power plants is gradually decreasing and production of shale oil has become more competitive as the world market prices of crude oil rise. As demand for shale oil products has increased significantly the wastes from the industry is increasing also. Thus it is important to find sustainable use for residuals from shale oil production. One option is synthesising geopolymeric materials which may be used as cements. This thesis focuses on less studied residual fly ash (hereinafter black ash) from the oil shale retorting using Petroter solid heat carrier technology. The aim of the current thesis is to investigate the synthesis of geopolymeric products from retorting ash (hereinafter black ash), formed in the production of shale oil using Petroter solid heat carrier technology.

## 2. GEOPOLYMERS

Geopolymers were first mentioned in 1950s when Victor Glukhovsky assumed that since the geological process of transformations of some volcanic rocks into zeolites takes place during formation of sedimentary rocks at low temperatures and pressure, it might be modelled and carried out in cementitious systems. These systems may ensure durability and other new useful properties. The founder of geopolymer science –Joseph Davidovits coined the term geopolymers as three-dimensional alumino-silicates that are formed at low temperature and short time by naturally occurring alumino-silicates (Davidovits 1988). Geopolymers may be broadly referred as „inorganic polymers“ (Duxson *et al.* 2007). Although they came upon the synthesis of geopolymers by observing the formation of zeolites, the two processes should not be confused since the resulting products are different in composition and structure. Unlike zeolites the geopolymeric products do not have stoichiometric composition and comprise mixtures of amorphous to semi-crystalline structure and crystalline Al–Si particles (Davidovits 1991).

Geopolymers consists of sialate (silicon-oxo-aluminate) network where $SiO_4$ and $AlO_4$ tetrahedra are alternately covalently linked by sharing all oxygen atoms (Figure 1). Positive ions such as $Na^+$, $K^+$ and $Ca^{2+}$, are present in the framework cavities to balance the negative charge of $Al^{3+}$ in IV-fold coordination.

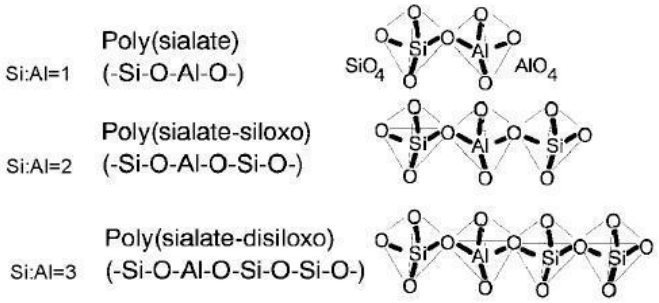


**Figure 1.** Types of polysialate monomers (Davidovits 2011).

Polysialates in geopolymers are chain and ring polymers, their empirical formula is displayed as $M_n(–(SiO_2)_z–AlO_2)_n \cdot wH2O$, where z is 1, 2 or 3, M is a monovalent cation such as $K^+$ or $Na^+$ and n is the degree of polycondensation. Geopolymerisation is an exothermic process which evolves through the condensation, step by step, from monomers to dimers, trimers and higher molecules (Figure 2). The starting monomers may be

siloxonate (Si–O–Si–O), sialate (Si–O–Al–O) and disiloxo-sialate (Si–O–Al–O–Si–O–Si–O) (Davidovits 2011). Other possible functional groups existing in the system are Al–O–Al groups (in high Al systems) and non bridging oxygen (NBO) of the form Si–OH, Si–O–Na+ or Al–OH. In addition, there may be small amounts of other less stable compounds, such as 5-coordinated Si species (Rees 2007).

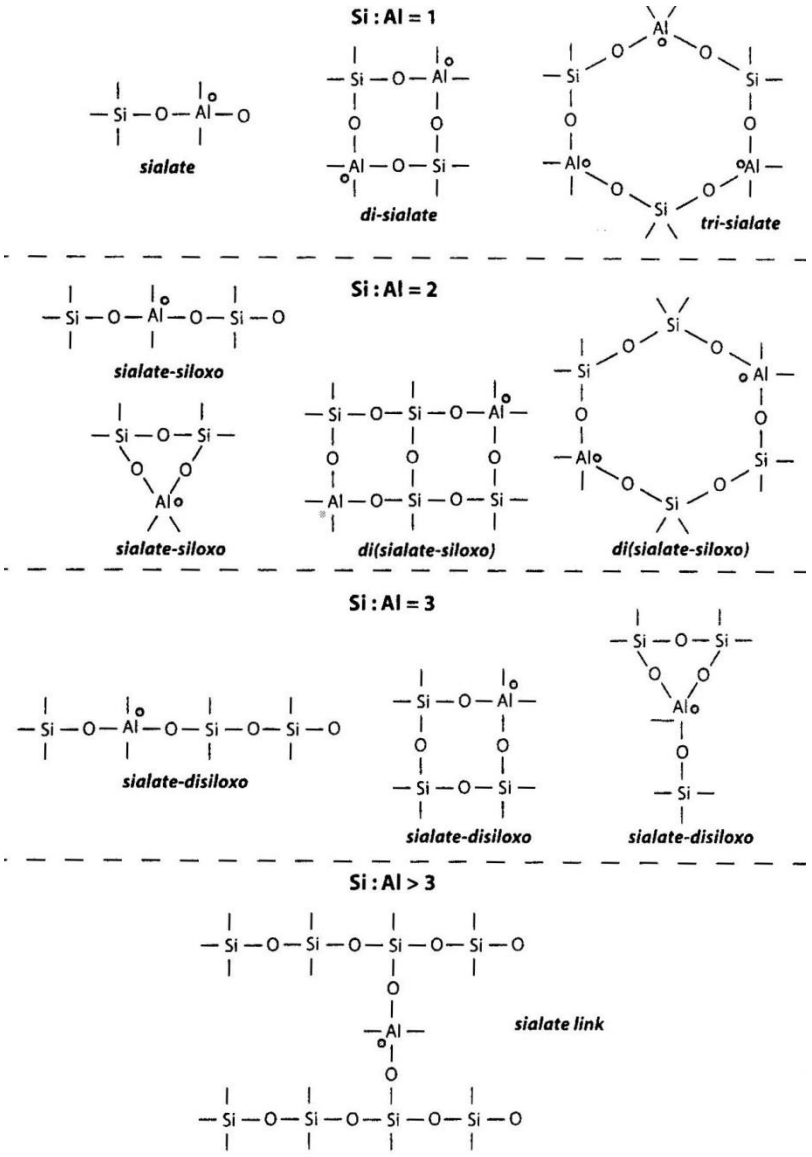


**Figure 2.** Different structures of polysialate (Davidovits 2011).

## 2.1. Synthesis of geopolymers

The simplyfied general mechanism of the synthesis of geopolymers is presented linearly below (Figure 3), but it should be noted that the actual processes are often coupled and occur simultaneously. Aluminosilicate raw material is dissolved in alkaline solution, through hydrolysis, aluminate and silicate species are released into aqueous phase forming a complex colloidal solution of silicate, aluminate and aluminosilicate species. Dissolution of amorphous aluminosilicates is rapid at high pH therefore a supersaturated aluminosilicate solution is formed. In supersaturated solution a gel is formed and aluminosilicate oligomers form networks in the aqueous phase by condensation. This process liberates water which was previously used for dissolution. Released water remains within pores in the gel, because of that the gel structure is referred to as bi-phasic: aluminosilicate network and water. For the formation of gel the solution must be concentrated since in diluted solutions there is no equilibrium between silicon and aluminium. The system continues to reorganize after gelation, more new strengthening bonds are created resulting in three-dimentional aluminosilicate network inherent to geopolymers (Duxson *et al.* 2007). It is important to note that generated geopolymers are not so structurally long-range ordered to be crystalline, their structure is amorphous or containing some level of short-range ordering.

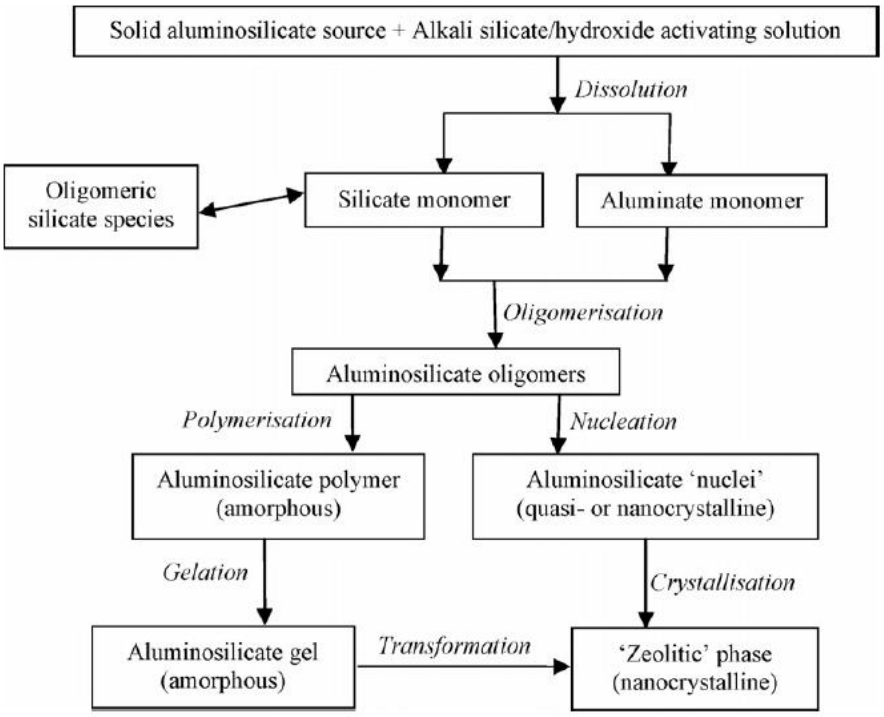


**Figure 3.** Synthesis of geopolymers, generalised mechanism (van Deventer 2007).

The content of CaO in source material appears to strengthen the geopolymer by forming amorphously structured Ca–Al–Si gel (Komnitsas & Zaharaki 2007). Several researches (Xu & Van Deventer 2000; Yip *et al.* 2005) have stated that calcium has a positive effect on the compressive strength of geopolymeric materials, because the microstructural porosity decreases and the resulting formation of amorphous structure Ca–Al–Si gel has a strengthening effect. Calcium content in the solid raw materials affects the process of geopolymerisation by providing extra nucleation sites for precipitation of dissolved species (Van Deventer *et al.* 2007). Presence of calcium partially determines the physical properties of the forming geopolymer. Excessive calcium and hydroxide ion content in initial synthesising solution causes precipitation of $Ca(OH)_2$ which later on reacts with $CO_2$ in the atmosphere forming calcite, $CaCO_3$, resulting in deterioration of the geopolymeric product.

## 2.1. Properties of geopolymers

The raw materials and processing conditions determinine the structure, chemical and physical properties of geopolymeric products. In macroscopic scale, geopolymers synthesised from different aluminosilicate sources may appear similar but their microstructure homogeneity and thus the physical, mechanical and chemical properties vary to a large extent (Subaer & van Riessen 2007).

Geopolymers are thermally stable up to 1000-1200 °C, also the early compressive strength is remarkable – up to 20 MPa. Surface hardness in Mohs scale is 4-7, they have high surface smoothness and precise mouldability. Other useful properites are freeze-thaw, sulphate and corrosion resistance. With these properties geopolymers can be useful tooling, moulding art objects, ceramics as well as building materials. Cements made of geopolymers show very low
shrinkage in air after drying, preventing thus formation of cracks. (Komnitsas & Zaharaki 2007)

# 3. ENERGY SECTOR WASTES IN ESTONIA

Direct combustion of kukersite oil shale, found in Estonia, releases enough energy to be used as a fuel. During burning the bituminous organic matter in kukersite releases energy but the other, inorganic matter is useless in the means of enegy production and turns into residual ash. Nearly half of the oil shale dry mass is left after combustion or shale-oil extraction as a solid residue. As Estonian oil shale is being the largest exploitable oil shale resource in the world (Teedumäe & Raukas 2006) the great amount of residual ash has a strong negative impact to the local environment. In Estonia the largest part of the mined oil shale is currently burned in thermal power plants for electricity and heat generation using pulverized fuel or circulating fluidized bed combustion. The remaining mined oil shale is retorted to produce shale oil and gas (Ots 2006).

Petroter technology uses the pyrolysis process to treat fine-grained oil shale (0-25 mm fraction) with a solid heat carrier. Through a mixture of oil shale and heated ash in the absence of air, the heating and destruction of organic matter contained in oil shale occurs followed by the emission of liquids and gases. The share of the fine-grained fraction in mined oil shale is approximately 70%.

The oil shale pyrolysis process is effected in a drum rotating reactor in the absence of air, at a temperature of 450–500°C, by mixing oil shale with hot ash (as a solid heat carrier). Vapour-gas mixture that appears in the reactor during the pyrolysis process is fed through several process vessels to be refined from ash and mechanical impurities, and is then subject to a distillation process to produce liquid products and gas with high calorific value. Liquid products are fed to other units for loading as final products or for further processing. Gas is fed to the heat power plant for heat and power production. Steam is fed to the heat power plant for power production. The by-products of this process include phenol water, flue gases and ash from thermal processing (black ash). (Viru Keemia Grupp 2014)

The American Society for Testing and Materials classifies fly ashes to class F and C. The first is produced by burning bituminous coals, the second is produced by burning lignite and subbituminous coals. The main difference between class F and C fly ash is the calcium

content, which is significantly higher in class C fly ash (ASTM 2008). By its composition the black ash is similar to class C fly ash. While low calcium (class F) fly ash is most commonly used for geopolymeric synthesis, extensive research has been aimed at high calcium (class C) fly ash. Previous works (Guo *et al.* 2010) have shown the potential of geopolymer production from C class fly ash creating good precontitions for the use of black ash as a raw material for geopolymer synthesis.

# 4. MATERIALS AND METHODS

The raw material – black ash was collected from the Petroter solid heat carrier retort at Viru Keemia Grupp AS (Kohtla-Järve, Estonia) The mineralogical and chemical composition of the ash is presented in Table 1 and 2 (Paaver 2014).

To understand the composition and the structure of the geopolymeric products, the following characterization techniques were used in this study: Attenuated Total Reflectance – Fourier Transform Infrared Spectroscopy (ATR-FTIR) and $^{29}Si$ solid state magic angle spinning nuclear magnetic resonance (MAS-NMR)

**Table 1.** Mineralogy of black ash.

| **Phase Name** | **Wt%** |
|---|---|
| Quartz | 11,71 |
| Orthoclase | 14,25 |
| Muscovite | 2,64 |
| Calcite | 26,81 |
| Dolomite | 8,52 |
| Lime | 2,08 |
| Periclase | 7,50 |
| C2S β (Belite) | 3,15 |
| Merwinite | 5,22 |
| Melilite | 4,19 |
| Wollastonite | 1,53 |
| Oldhamite | 3,59 |
| Anhydrite | 1,10 |
| Hematite | 1,09 |
| Magnetite | 0,94 |
| Amorpus phase | 5,7 |

**Table 2.** Chemical composition of black ash.

| **Oxide** | **Wt%** |
|---|---|
| $SiO_2$ | 21,23 |
| $Al_2O_3$ | 5,27 |
| $TiO_2$ | 0,16 |
| $Fe_2O_3$ | 3,65 |
| MnO | 0,07 |
| CaO | 31,89 |
| MgO | 8,15 |
| $Na_2O$ | 0,11 |
| $K_2O$ | 2,58 |
| Cl | 0,34 |
| $P_2O_5$ | 0,11 |
| S | 1,97 |

## 4.1. Synthesis of geopolymer samples

Geopolymer samples were prepared by mixing the ash material with the activating solution, in ratios based on previous works on alkali activation of class C high calcium fly ash (Guo *et al.* 2010, Roy *et al.* 1996) which chemical composition is compareable to black ash. The activating agents used in this study were water, sodium hydroxide, sodium disilicate with $SiO_2/Na_2O$ molar ratio 2,72 and mixture of sodium hydroxide and sodium disilicate with $SiO_2/Na_2O$ molar ratio 1,5.

As the ash material possesses cementitious and pozzolanic properties (Sedman 2013) the first series of samples were prepared using deionized water and were used as a reference for the determination of the degree of polymerisation reactions in alkaline medium. In the second series of samples the raw material was activated with 5 molar sodium hydroxide solution (Roy *et al.* 1996, US patent 5565028) to prevent the formation of ettringite which would significantly affect the strength of the material and other activating agents. A sodium disilicate solution with a molar ratio of $SiO_2/Na_2O$ 2,72 and water content of 47,4% (w/w) was used to prepare the third series of samples. The fourth series was prepared using a sodium disilicate solution in which the molar ratio of $SiO_2/Na_2O$ was modified to 1,5 after Guo *et al.* 2010 and Davidovits 2013. All sodium silicate based activator solutions were prepared in a way that the $Na_2O$ concentration in the additive was 10% (w/w) so as to normalise the amount of soluble silicate in the mixtures. Corresponding ratios of *$H_2O/ash$*, *$Na_2O/ash$* and *$SiO_2/Na_2O$* are given in Table 3.

**Table 3.** Mix designs of the geopolymer samples.

| Sample | | $H_2O$/ash | $Na_2O$/ash* | $SiO_2/Na_2O$* |
|---|---|---|---|---|
| E | BA + $H_20$ | 0,5 | | |
| B | BA + 5M NaOH | 0,5 | 0,09 | |
| A | BA + sodium disilicate | 0,5 | 0,1 | 2,72 |
| C | BA + sodium disilicate | 0,5 | 0,1 | 1,5 |

*$SiO_2/Na_2O$ and $Na_2O$ values represent the alkaly activator components and not the overall chemical composission of the mixtures.

After the addition of activating solution to the black ash, the mixtures were poured in cylindrical mold with a diameter of 23 mm and height of 35 mm. To ensure that the container was filled homogeneously the samples were placed on a vibrating stand for 1 minute. The samples were then placed to dry at ambient temperatures. Alltogether 45 samples were prepared, nine with each activating solution.

After 7, 28 and 90 days 3 samples of each type were crushed. The strongest was picked through compression strength test and grounded fine in a mortar for further analysis.

## 4.2. Attenuated Total Reflectance – Fourier Transform Infrared spectroscopy (ATR-FTIR)

In the current thesis the source material and grounded geopolymer samples after 7, 25 and 90 days of curing were analysed with Attenuated Total Reflectance – Fourier Transform Infrared Spectroscopy (ATR-FTIR). The ATR-FTIR spectra of the samples were collected using a „Smart Orbit“ diamond ATR-microanalysator with CsI optics attached to Thermo Scientific Nicolet 6700 FT-IR spectrometer which allows measuring between 10000-55 $cm^{-1}$. Absorbance spectra were collected from 225-4000 $cm^{-1}$ at a resolution of 4 $cm^{-1}$ with 128 scans. The spectrometer was controlled and the spectra processed in Thermo Electron’s OMNIC program.

ATR-device is based on a total internal reflection principle. The crystal of ATR is covered with sample and the infrared light is directed from the inside of the crystal on the surface which is in contact with the crystal. The infrared light is directed at an angle that the phenomenon of total reflectance occurs. Part of the infrared beam reaches to the sample what is on the ATR-crystal and is partly absorbed by molecules and converted into energy of molecular vibration; when the radiant energy matches the energy of a specific molecular vibration, absorption occurs. The intensity of the infrared light which reflects back from the sample is registered and compared with the intensity of the infrared which reflects back if there is no sample on the crystal, hence the optical absorbance is found. The total internal reflection phenomenon occurs only if the ATR-cristal has higher refractive index than the sample. ATR-FTIR spectroscopy is a fast and relatively simple method. The

samples do not need specific pretreatment and samples with different consistency and state can be analysed. The advantage of ATR attachment to FTIR spectroscope is that the amount of the sample may be very small. One important aspect is that the contact between sample and crystal must be good. (Teearu 2009)

ATR-FTIR allows to identify different chemical bonds in the sample – different bonds absorb distinct infrared wavelengths. Materials are characterised by the vibrations of the bonds, which involves streching, bending and other deformations. Bonds can stretch in-phase (symmetrical stretching) or out-of-phase (asymmetric stretching). One drawback is the complexity of interpreting the ATR-FTIR spectrum, as the bands from fundamental vibrations and bands from overtone vibations are hardly distinguished. (Rees 2007)

## 4.3. Magic Angle Spinning - Nuclear Magnetic Resonance spectroscopy (MAS-NMR)

Solid state $^{29}$Si MAS-NMR measurements from source material and grounded samples after 28 and 90 days of curing were made in The National Institute of Chemical Physics and Biophysics (Tallinn, Estonia) by Senior Research Fellow, PhD Ivo Heinmaa. $^{29}$Si MAS-NMR spectrometer used in this thesis was a Bruker AVANCE-II NMR spectrometer attached to 8,5 T magnet ($^{29}$Si resonance frequency 71,4 MHz). About 1,8 g of each sample was rotated at 5 kHz in 10 mm o.d. zirconia rotors using home-built MAS probe with single-pulse and a relaxation delay of 100 s. Number of scans was 800 to 1600.

Magic Angle Spinning - Nuclear Magnetic Resonance spectroscopy (MAS-NMR) is a method which allows the measurement of the electron density around each nucleus in a *chemical environment* in solid state, giving information on how atoms are linked to each other in the sample. MAS-NMR is the most effective method for determing the structure of amorphous solids such as geopolymers synthesised from fly ash.

NMR can be used only if the sum of protons and neutrons of an atom in the molecule is an odd number. When the proton is placed in an external magnetic field, the spin vector of the particle aligns itself with the external field, just like a magnet would. Each spin aligns in

one of the two possible orientations: there is a low energy configuration and a high energy configuration. At room temperature, the number of spins in the lower energy level, $N^+$, slightly outnumbers the number in the upper level, $N^-$.

The signal in NMR spectroscopy results from the difference between the energy absorbed by the spins which make a transition from the lower energy state to the higher energy state, and the energy emitted by the spins which simultaneously make a transition from the higher energy state to the lower energy state. The signal is thus proportional to the population difference between the states. NMR is a rather sensitive spectroscopy method since it is capable of detecting these very small population differences. It is the resonance, or exchange of energy at a specific frequency between the spins and the spectrometer, which gives NMR its sensitivity. (Hornak 1996) The distribution of particles between the lower and upper enery level depends on gyromagnetic ratio ($\gamma$) and force of exteral magnetic field ($B_0$) (Equation 1).

$$\frac{N^-}{N^+} = e^{-c\gamma B_0} \approx 1 - c\gamma B_0 \quad (1)$$

For example in case of hydrogen nuclei if $B_0$=4,69 T, for 1 000 000 particles in the upper energy level there is 1 000 033 particles in the lower energy level. The difference is only 33 ppm, therefore the measured signal is very weak. (Leito 2013)

When an atom is placed in a magnetic field, its electrons circulate about the direction of the applied magnetic field. This circulation causes a small magnetic field at the nucleus which opposes the externally applied field. The electron density around each nucleus in a molecule varies according to the types of nuclei and bonds in the molecule. The opposing field and therefore the effective field at each nucleus will vary. This is called the *chemical shift* phenomenon. The *chemical shift* of a nucleus is the difference between the resonance frequency of the nucleus and a standard, relative to the standard. This quantity is reported in ppm and given the symbol delta, $\delta$. (Hornak 1996)

### 4.3.1. $^{29}$Si MAS-NMR spectroscopy

$^{29}$Si MAS NMR spectroscopy is a useful tool for describing the nanostructure of geopolymers. In $^{29}$Si MAS-NMR the chemical shift δ depends on the chemical environment of the $^{29}$Si nucleus. $^{29}$Si chemical shift is dependent on the degree of condensation of the $SiO_4$ unit, with increasing condensation corresponding to more negative δ. Furthermore, the NMR analysis allows quantitative determination of Si components because the intensity of signal is proportional to the number of $^{29}$Si nuclei present. (Davidovits 2011)

To describe the structural units in aluminosilicates the conventional notation is Qn(mAl), with „n“ representing the covalence number of the silicon center with values of 0,1,2,3 or 4. In case of Q0 the silicon is in isolated mono group. Q1 represents disilicates and chain end groups. Middle groups in chains are marked with Q2. Q3 notes branching silicon sites and Q4 three-dimensional cross-linked sites. The letter „m“ represents the number of Al surrounding silicon tetrahedra, that is the number of Si–O–Al links in sialate unit. Possible Qn(mAl) chemical structures and corresponding $^{29}$Si MAS-NMR chemical shift δ values are given in Figure 4.

After the determination and quantification of the silicon species the mean chain length (MCL) of silicate structures comprising of $SiO_4/AlO_4$ tetrahedra can be estimated from the relative fractions of the different Q–species according to Equation 2 (Richardson *et al.* 1997).

$$MCL = \frac{Q1+Q2+\frac{3}{2}Q2(1Al)}{\frac{1}{2}Q1} \quad (2)$$

| $Q_n$ | -δ (ppm) | $Q_n$(1Al) | -δ (ppm) | $Q_n$(2Al) | -δ (ppm) | $Q_n$(3Al) | -δ (ppm) | $Q_n$(4Al) | -δ (ppm) |
|---|---|---|---|---|---|---|---|---|---|
| $Q_0$  | 66 to 73 | | | | | | | | |
| $Q_1$  | 76 to 83 | $Q_1$(1Al)  | 75 | | | | | | |
| $Q_2$  | 86 to 91 | $Q_2$(1Al)  | 85 | $Q_2$(2Al)  | 80 | | | | |
| $Q_3$  | 95 to 101 | $Q_3$(1Al)  | 95 | $Q_3$(2Al)  | 90 | $Q_3$(3Al)  | 85 | | |
| $Q_4$  | 103 to 120 | $Q_4$(1Al)  | 97 to 105 | $Q_4$(2Al)  | 92 to 99 | $Q_4$(3Al)  | 88 to 94 | $Q_4$(4Al)  | 83 to 87 |

**Figure 4.** Qn(mAl) chemical structures and corresponding chemical shift δ values (Davidovits 2011).

# 5. RESULTS AND DISCUSSION

To apprehend the ATR-FTIR and $^{29}$Si MAS-NMR spectum of material, some knowledge about the composition and structure is necessary. Since black ash contains a significant amount of calcium which is not essential in any part of a basic geopolymeric structure, it is proposed that if sufficient calcium is added to a geopolymeric system, a calcium silicate hydrate (C–S–H) based cementitious material may form instead.

Figure 5 shows the likely reaction products formed when calcium is added to a geopolymeric system (Yip *et al.* 2005).

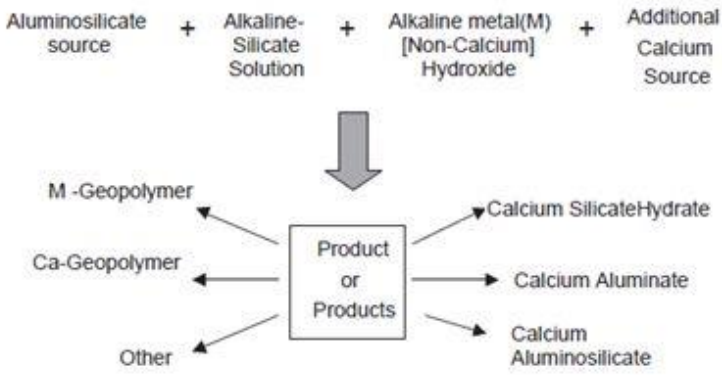


**Figure 5.** Reaction products of geopolymeric system when calcium is added (Yip *et al.* 2005).

## 5.1. ATR-FTIR spectra of geopolymers

To understand the FTIR spectrum of geopolymeric material, we should know that geopolymer is a hydrous alkali aluminosilicate, with a tetrahedral silicate network with a number of the tetrahedral positions occupied by $Al^{3+}$ in four fold coordination, charge stabilised by an alkali cation. Also there may be some Al–O–Al groups and non-bridging oxygens of the form Si–OH, $Si–O^{-}$ $Na^{+}$ or Al–OH existing in the system. It should be noted that any factor which strains, lengthens or alters the Si–O–Si bond will affect the FTIR spectra (Rees 2007). The FTIR spectra of silicates are very sensitive to the substitution of ions of different charge, but much less sensitive to substitution of ions of the same charge. The substitution of trivalent ions into the tetrahedral positions in a silicate network causes

the main Si–O stretching band (1100-900cm$^{-1}$) to shift to lower wavenumbers due to the average increase in the (Si, Al)–O bond length and the increased ionic character of the bond (Rees 2007). However, the remaining Si–O bonds in what were previously the pairing silicate tetrahedra may experience an increase in strength due to the resulting change in polarisation at the O site on the Si–O–Al linkage, leading to higher wavenumber contributions to the main Si–O band and consequent broadening of the band around 970 cm$^{-1}$. In FTIR spectrum crystalline materials present sharp well-defined bands as amorphus phases give broad, poorly defined bands (Fernández-Carrasco 2012).

### 5.1.1. ATR-FTIR spectra of black ash geopolymers

Figures 6-9 display ATR-FTIR spectra of initial black ash (red), and differently activated samples after 7 (blue), 28 (green) and 90 (purple) days. Multiple changes in the FTIR spectra between the original black ash and activated samples can be observed in all sample series. New bands around 3300-3400 cm$^{-1}$ and 1640 cm$^{-1}$, reprecenting O–H streching and bending vibrations in $H_2O$ become visible in every sample. The sharp bands at 1795cm$^{-1}$; 1400 cm$^{-1}$; 870, cm$^{-1}$ and 712 cm$^{-1}$ represent C–O vibrations in $CO_3^{2-}$ ion (García-Lodeiro *et al.* 2007), confirming the presence of calcite which was also observed in X-ray diffraction analysis (appendix A). Tough these bands are prominent in every spectrum they have little significance in this research. The shoulder at 1120 cm$^{-1}$ and low band at 594 cm$^{-1}$ in the original black ash spectrum correspond to the streching and bending of S–O bond of $SO_4^{2-}$ in anhydrite (Fernández-Carrasco 2012) which is also in correlation with mineralogical composition (Appendix A). The relevant peaks indicating to Si functional groups remain between 400-1200 cm$^{-1}$.

The FTIR spectra of water activated black ash (Figure 6) show a band around 970 cm$^{-1}$ associated with the Si–O–Si (Si–O–Al) (Yu *et al.* 1999) asymmetric streching vibrations in $SiO_4$ tetrahedra. According to Yu *et al.* 1999 this band represents Q2 silicon site. The band shifts to higher wavenumbers after 7 days and then shifts back to lower wavenumbers, indicating that initially formed structures deform in time. The band at 1110 cm$^{-1}$ is a combination of Si–O stretching vibrations from amorphous silicate phases assosiated with Q3 silicon sites (Rees 2007) and S–O vibrations in $SO_4^{2-}$, arising from different sulfate

minerals like gypsum and ettringite in the sample (Appendix A). The band at 1110 $cm^{-1}$ is likely the result of dissolution and depolymerisation of the amorphous glass phase present in the source material and subsequent polymerisation as braching Q3 silicon species.

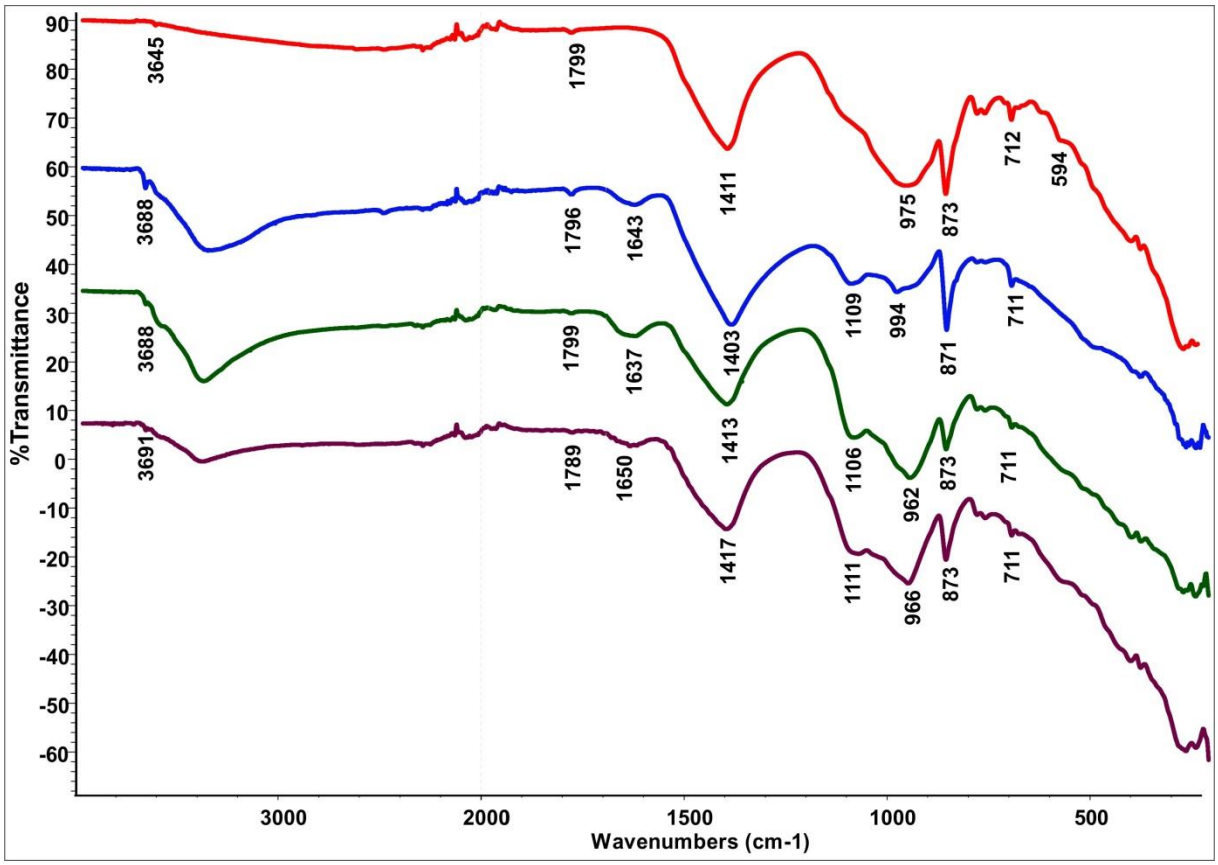


**Figure 6.** ATR-FTIR spectra of black ash (red) and $H_2O$ activated black ash after 7 (blue), 28 (green) and 90 (purple) days.

The FTIR spectra of initial black ash and samples prepared using sodium disilicate solution with $SiO_2/Na_2O$ ratio 2,72 (Figure 7) show a Si–O–Si streching band around 960 $cm^{-1}$ corresponding to Q2 silicon site. The main band in original black ash is centered at 975 $cm^{-1}$, after 7 days the band has shifted to lower wavenumbers (959 $cm^{-1}$) which referrs that during alkali-activation, every bridging oxygen atom of initial aluminosilicate is replaced by two non-bridging oxygen atoms with negative charge – the process is called depolymerisation. Through that process the $TO_4$ (T = Si or Al) tetrahedras within the network have become more isolated with increasing alkali concentration. Consequently, the T–O bonds in the tetrahedra should possess lower molecular vibration force constants, resulting in shift of the infrared band to smaller wavenumbers. (Lee & van Deventer 2003)

After 28 and 90 days it appears that the band shifts progressively to higher wavenumbers from 959 $cm^{-1}$ to 962 $cm^{-1}$ and to 979 $cm^{-1}$ which points out that the material continuously polymerises and the bonds are strengthening and polymer is lengthening (see Chapter 5.1).

Spectra of black ash activated with sodium disilicate solution with $SiO_2/Na_2O$ ratio 1,5 (Figure 9) represents the same shift of Si–O–Si (Si–O–Al) band to lower wavenumbers at the beginning and later shift to greater wavenumbers, indicating to the same tendency of polymerisation.

Also it is observed that in the 7 day spectrum of samples which have additional $Na^+$ (Figures 7-9) the Si–O–Si peaks have shifted to lower wavenumbers than in the spectra of $H_2O$ activated ash. This phenomenon is in agreement with the previous studies (Rees 2007) stating that the higher $Na^+$ content leads to the shift of the Si–O–Si band to lower wavenumbers.

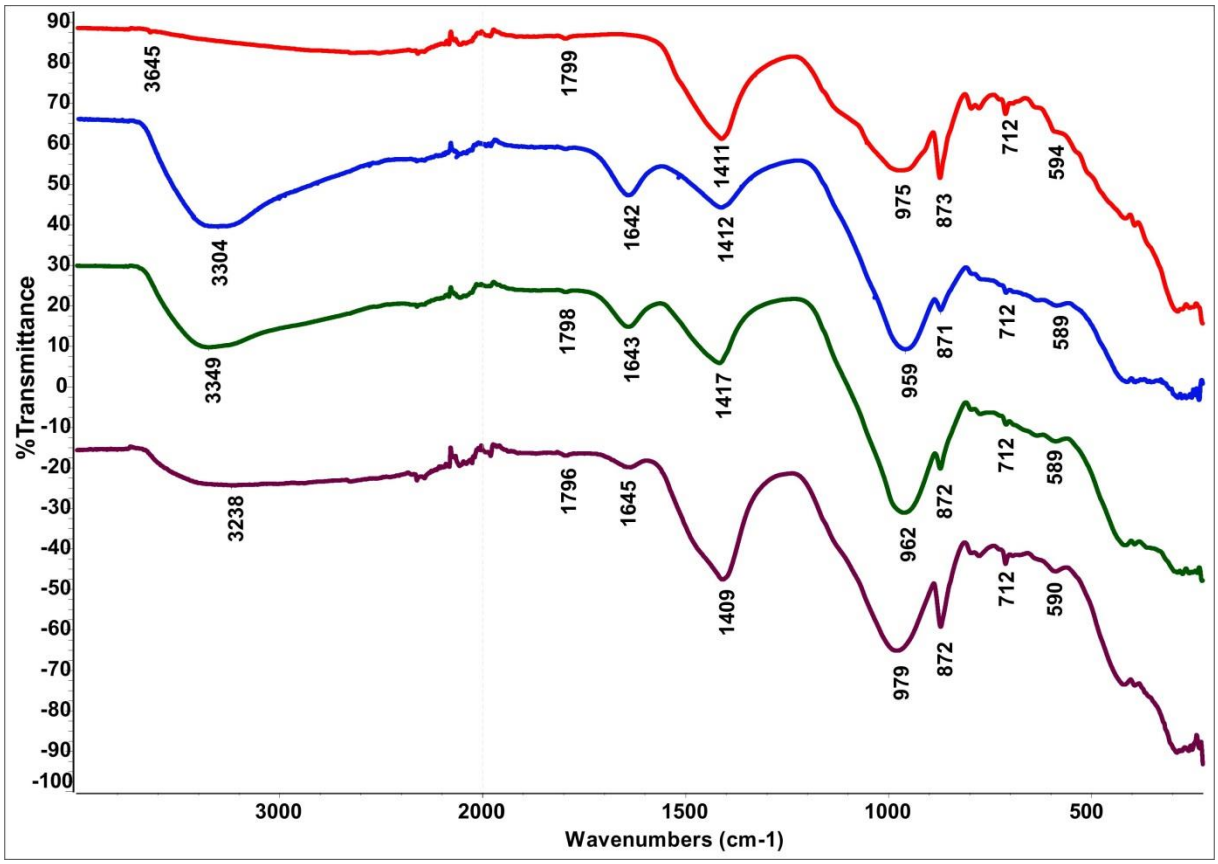


**Figure 7.** ATR-FTIR spectra of black ash (red) and sodium disilicate with $SiO_2/Na_2O$ 2,72 activated black ash after 7 (blue), 28 (green) and 90 (purple) days.

Figure 8 displays infrared spectra of NaOH activated black ash sample, there one sharp band at at 3640 $cm^{-1}$ is present, characteristic to O–H stretching in portlandite ($Ca(OH)_2$) (García-Lodeiro *et al.* 2009) The main band is split into two components, around 945 $cm^{-1}$ and around 990 $cm^{-1}$ that are associated with Si–O–Si and Si–O–Al streching vibrations in Q2(1Al) and Q2 silicon site respectively (Lecomte *et al.* 2006). The increase in intensity of the 990 $cm^{-1}$ band after 28 days shows that the relative abundance of Q2 silicon sites has increased. Due to the sharpness and well-defined shape of these bands, the corresponding silicon sites are likely not assosiated with one predominant amorphous phase and represent in themselves different silicate structures. The band at 1117$cm^{-1}$ can be attributed to S–O streching vibrations in gypsum (Fernández-Carrasco *et al.* 2012) and Si–O vibrations of amorphous silicate phases, similar to water based samples. The shifting of the band to a higher freguency of 1126 $cm^{-1}$ after 90 days can be assosiated with polycondensation of the silicon species in the amorphous phase. The band at 670 $cm^{-1}$, not present in other samples, consists of S–O bending vibrations in gypsum.

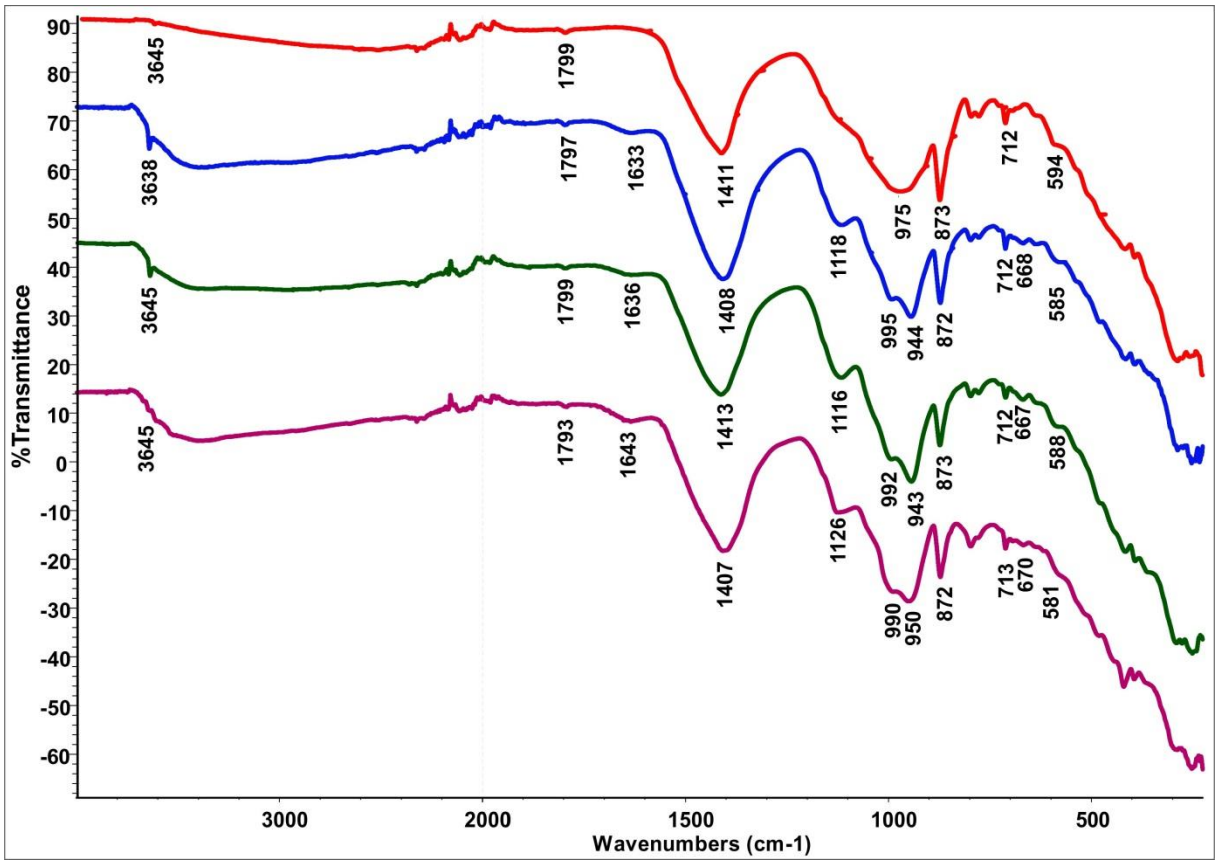


**Figure 8.** ATR-FTIR spectra of black ash (red) and NaOH activated black ash after 7 (blue), 28 (green) and 90 (purple) days.

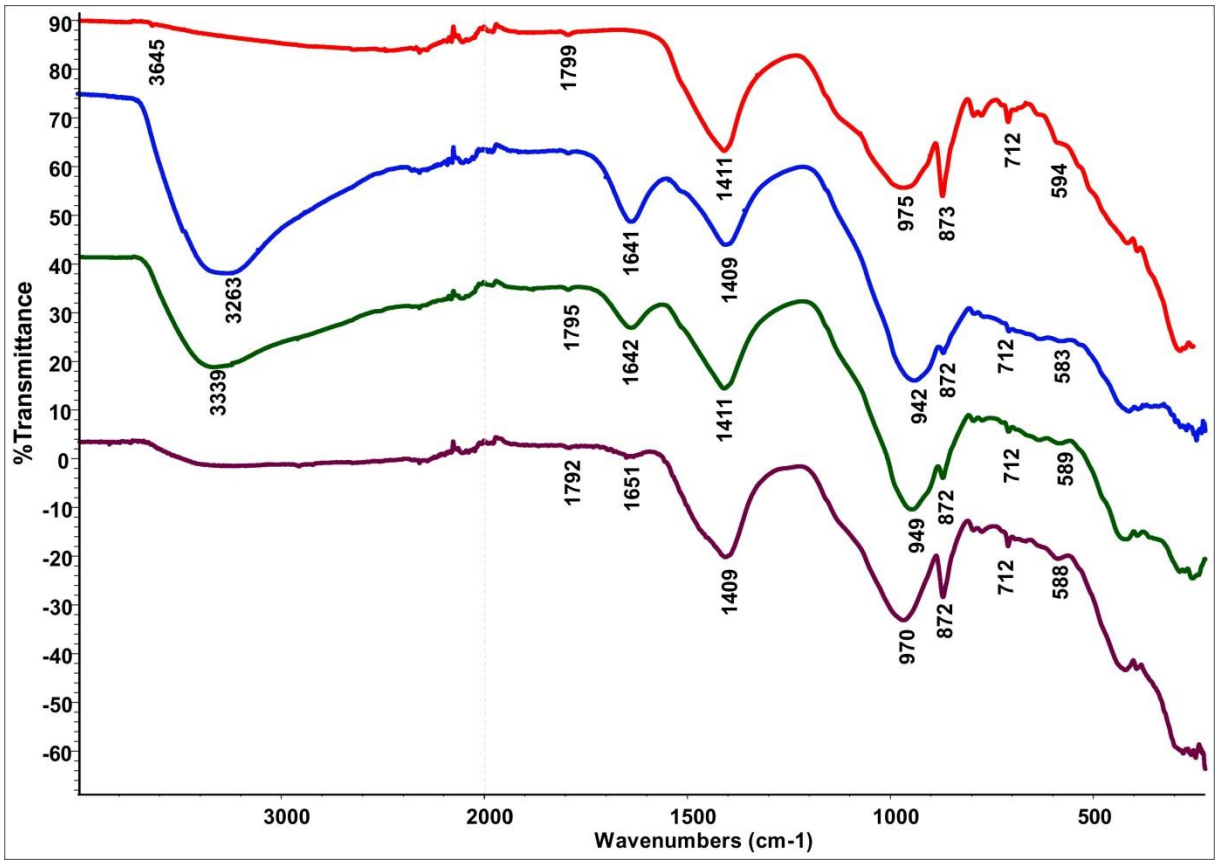


**Figure 9.** ATR-FTIR spectra of black ash (red) and sodium disilicate solution with $SiO_2/Na_2O$ ratio 1,5 activated black ash after 7 (blue), 28 (green) and 90 (purple) days.

## 5.2. $^{29}$Si MAS-NMR spectra of black ash geopolymers

The spectra of initial black ash is shown in Figure 10. The spectra shows a broad peak in the range from –80 to –105 ppm. This peak can be appointed to the different silicon sites in amorphus ash glass (Reinik *et al.* 2007). The resonance line at –72,69 ppm arise from belite and alite (Mägi *et al.* 1984), the peak at –108,11 ppm can be assigned to quartz (Lippmaa *et al.* 1980). The contributions of every peak to total spectrum are given in Appendix B.

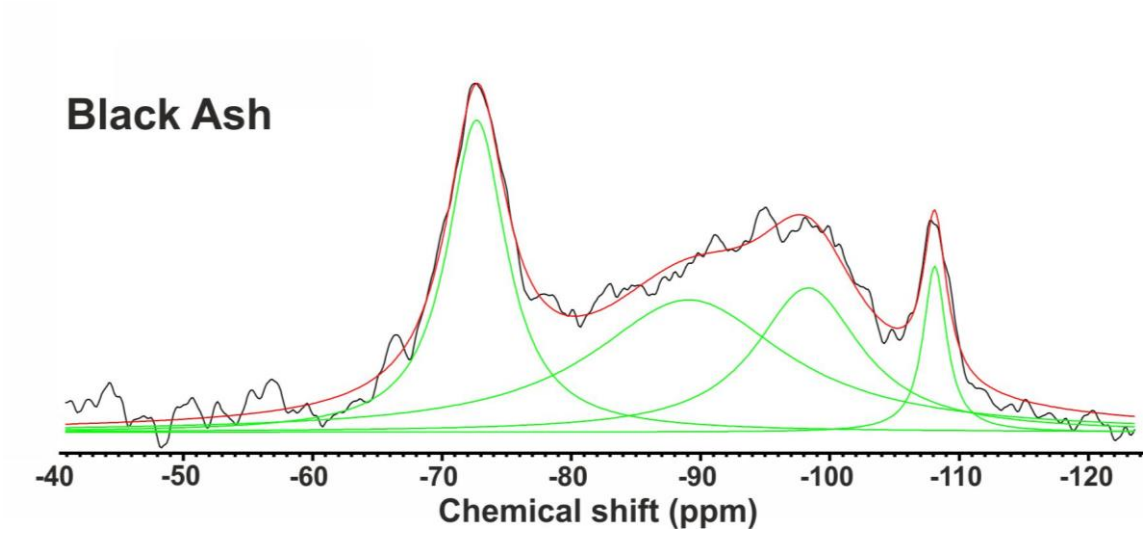


**Figure 10.** $^{29}$Si MAS-NMR spectrum of untreated black ash.

Figure 11 shows the 28 day $^{29}$Si MAS-NMR spectrum of black ash activated with water. Locations and proportions of corresponding peaks are shown in Table 4. The spectrum presents number of peaks compared to initial black ash spectrum. The belite and alite peak intensity has lowered and quartz peak shows no change. New resonance lines at –79,89; –85,2; –95,4 and –100,95 ppm can be appointed to Q1, Q2 (Komarineni *et al.* 1985), amorphous phase dominated by Q3 and Q3 (Davidovits 2011) silicon sites respectively.

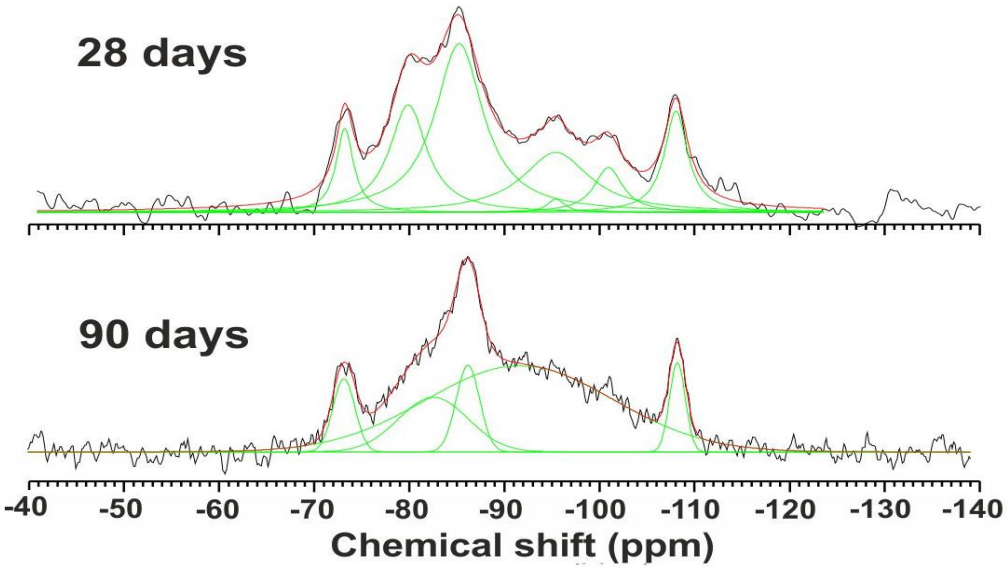


**Figure 11.** $^{29}$Si MAS-NMR spectra of water activated black ash after 28 and 90 days.

**Table 4.** Locations and proportions of peaks in $^{29}$Si MAS-NMR spectrum of water activated black ash and original black ash.

| | Belite/ Alite | Q1 | Q1 | Q2 | Q2 | Glass | Glass | Amorph (Q3) | Glass | Q3 | Quartz |
|---|---|---|---|---|---|---|---|---|---|---|---|
| Days/ppm | -73,13 | -79,89 | -82,54 | -85,2 | -86,16 | -89,1 | -91,63 | -95,4 | -98,3 | -100,95 | -108 |
| Bash | 0,29 | | | | | 0,41 | | | 0,24 | | 0,06 |
| E28 | 0,07 | 0,19 | | 0,38 | | | | 0,2 | | 0,06 | 0,11 |
| E90 | 0,06 | | 0,15 | | 0,08 | | 0,65 | | | | 0,06 |

After 90 days it seems that initially formed structures have disintegrated and the spectrum has taken a shape compareable to the spectrum of initial black ash. The peaks of Q1 and Q2 silicon sites are still present at –82,54 and –86,16 ppm but their intensities have lowered. A new major resonance line has appeared, centered at –91,63 ppm which is similarly to original black ash and appointed to the different silicon sites in amorphus ash glass. The NMR spectra of water activated black ash is in accordance with FTIR spectra (Figure 6) showing that structures formed at the beginning are depolymerising and dissapearing.

Figure 12 shows the NMR spectra of black ash activated with sodium disilicate $SiO_2/Na_2O$ 2,72, after 28 days. Locations and proportions of corresponding peaks are shown in Table 5. Compared to original black ash the peak respective to belite and alite has vanished, the peak of quartz is flattened and one prominent peak has risen in the spectra. Along smaller peaks at around –108,7 and –108,4 ppm which have been assigned to Q4 silicon sites and quartz respectively (Lippmaa *et al.* 1980) one broad peak can be distinguished which resonance is characteristic of semi-crystalline C–S–H gel. However the C–S–H gel in the sodium disilicate activated sample is different from the binding gel phase in Portland cement. The peak is centred approximately at –89 ppm originating from the Q2 middle groups (Davidovits 2011). The predominance of Q2 middle groups indicate that most of the silicate tetrahedra are chain mid-members. According to Lecomte *et al.* 2006, the $^{29}$Si MAS-NMR spectra of usual Portland cement shows a peak resonating at –80 and –86 ppm previously assigned to Q1 end groups and Q2 middle groups, meaning that the silicate groups are organized in shorter linear finite chains. Also the more negative

chemical shift of the sodium disilicate activated black ash sample reflects to significantly longer aluminosilicate chains than in Portland cement.

The other possible interpretation according to Lecomte *et al.* 2006 who used metakaolin and alkali-activated slag to synthesise geopolymers and got comparable $^{29}$Si MAS-NMR results as in this thesis, is that the broad peak centred approximately at −89 ppm, is consistent with chain branching sites (Q3 units) and three-dimensional cross-linked sites (Q4 units), both with substantial Al substitution for Si. Indicative of a highly polymerised structural aluminosilicate framework.

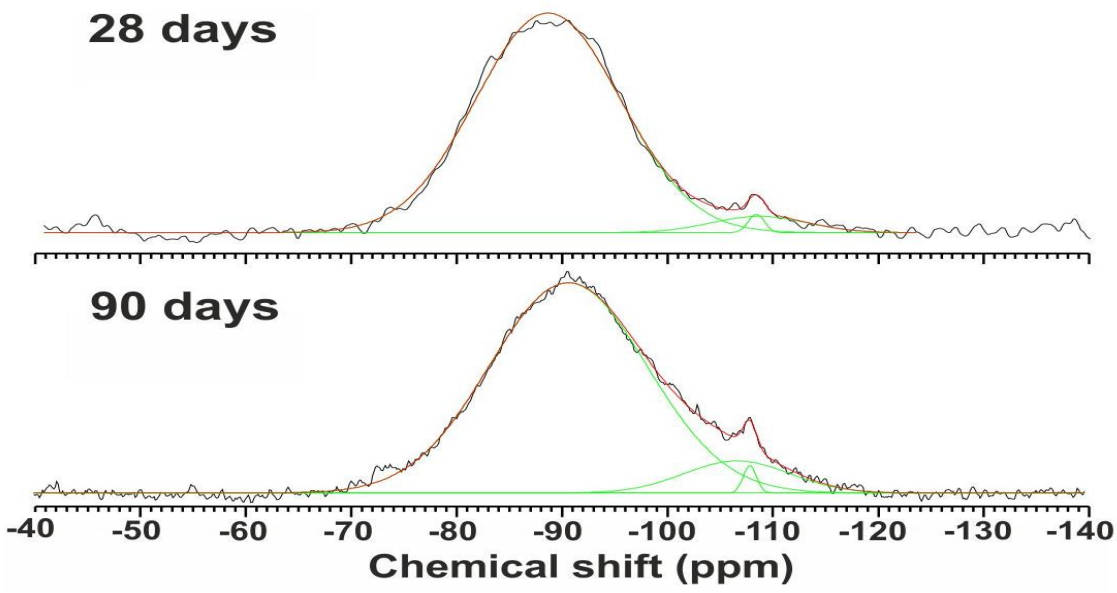


**Figure 12.** $^{29}$Si MAS-NMR spectra of sodium disilicate with $SiO_2/Na_2O$ 2,72 activated black ash after 28 and 90 days.

**Table 5.** Locations and proportions of peaks in $^{29}$Si MAS-NMR spectrum of sodium disilicate with $SiO_2/Na_2O$ 2,72 activated black ash and original black ash.

| | Belite/Alite | CSH (Q2) | Glass | CSH (Q2) | Glass | Q4 | Q4 | Quartz |
|---|---|---|---|---|---|---|---|---|
| Days/ppm | -72,69 | -88,7 | -89,1 | -90,6 | -98,3 | -106,6 | -108,7 | -108 |
| Bash | 0,29 | | 0,41 | | 0,24 | | | 0,06 |
| 28 | | 0,94 | | | | | 0,05 | 0,01 |
| 90 | | | | 0,9 | | 0,09 | | 0,01 |

When comparing the 28 and 90 day sample spectrums it can be noted that in the 90 day spectrum the main peak is shifted towards more negative chemical shifts and the less sharp Si–O–Si Q4 silicon site peak has increased in intensity. This indicates that the polymerisation process continues – the alumosilicate chains are rearranging and lengthening for a long time after the initial activation. Thus the $^{29}$Si MAS-NMR is in accordance with the results from ATR-FTIR.

The $^{29}$Si MAS-NMR spectra of NaOH activated black ash after 28 days is shown in Figure 13. Locations and proportions of corresponding peaks are shown in Table 6. Compared to the spectra of the original black ash sample the difference is noticeable. The relative intensity of the resonance line is increased, the belite and alite peak has decreased and the different silicon sites attributed to amorphus ash glass are no longer present or decreased in intensity. The spectra presents resonance lines at –78,92; –81,74; –84,01 and –100,8 ppm which arise from the silicon sites Q1, Q2(1Al), Q2 and Q3 (Lippmaa *et al.* 1980), respectively. The broad resonance line at –96,5 ppm may be associated with amorphous silicate phase formed during the hydration of the black ash. The peak at –108,02 ppm belongs to quartz. The spectra shows that most of the initial glass phases in the black ash have dissolved, and formed a silicate structure where the Q1 silicon site is at the end of the silicate chain and Q2 is linear middle groups in the silicate chain. According to Equation 1, the mean chain length of silicate structures is 5,3. Q2(1Al) is the chain middle group where one of the two neighbouring tetrahedra contains aluminium ion and Q3 is a branching silicate site where one $SiO_4$ tetrahedron links together two chains, meaning that the site has three nearest neighbour $SiO_4$ tetrahedras. The presence of Q2(1Al) peak in NMR spectra is also in correspondence with the FTIR spectrum of NaOH activated black ash (Figure 8).

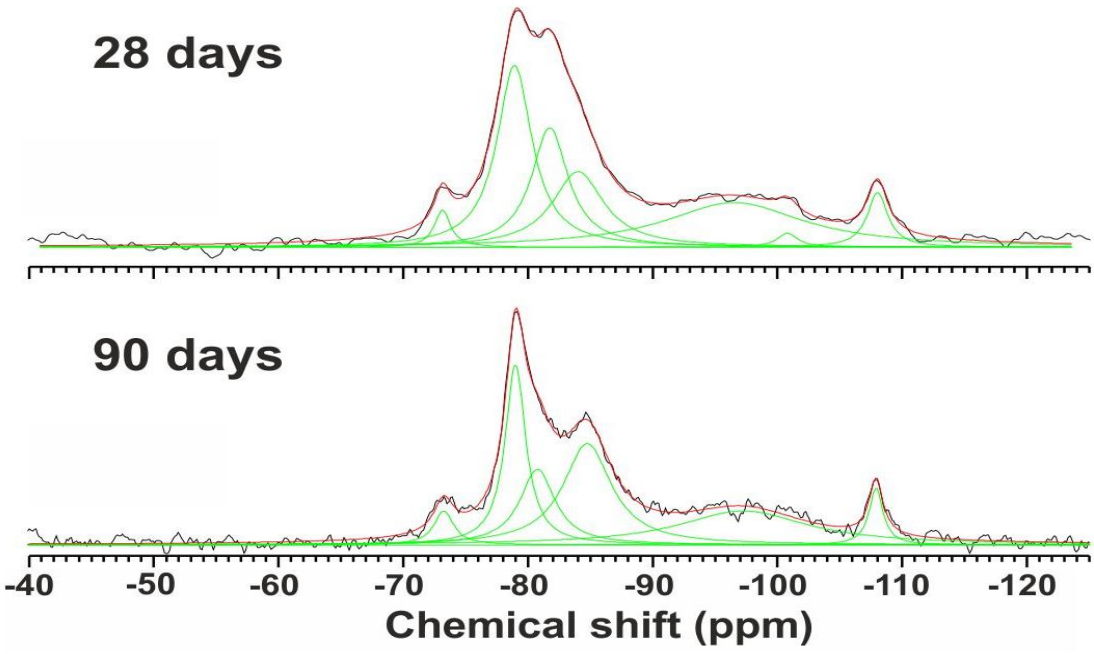


**Figure 13.** $^{29}$Si MAS-NMR spectra of NaOH activated black ash after 28 and 90 days.

**Table 6.** Locations and proportions of peaks in $^{29}$Si MAS-NMR spectrum of NaOH activated black ash and original black ash.

| | Belite/Alite | Q1 | Q2(1Al) | Q2 | Glass | Glass | Glass | Glass | Q3 | Quartz |
|---|---|---|---|---|---|---|---|---|---|---|
| Days/ppm | -73,13 | -78,92 | -81,74 | -84,01 | -89,1 | -96,5 | -97,3 | -98,3 | -100,8 | -108 |
| Bash | 0,29 | | | | 0,41 | | | 0,24 | | 0,06 |
| B28 | 0,03 | 0,28 | 0,19 | 0,17 | | 0,27 | | | 0,01 | 0,05 |
| B90 | 0,04 | 0,22 | 0,16 | 0,29 | | | 0,26 | | | 0,02 |

After 90 days since the activation with NaOH the spectrum shows a peak shift of the amorphous silicate phase to lower values. The realtive intensity of the peak corresponding to Q1 silicon site has decresed. At the same time the relative intensity of the peaks attributed to Q2 sites increase, meaning that there are more Si–O–Si–O–Si middle groups and the mean chain length of the silicate structures has increased to 6,8. These features correspond to the lengthening of the silicate chains and show that the material is continuously polymerizing after 28 days. The presence of the amorphous phase arising

from the hydration of the glass phases reveal that 5M NaOH solution was not sufficient to dissolve the entire amorphous phase present in the source material. The relatively short chain lengths of the silicate structure indicate that the dissolved silicon species arising from the alkaly reaction are only weakly polymerised.

Figure 14 shows the $^{29}$Si MAS-NMR spectra of sodium disilicate with $SiO_2/Na_2O$ 1,5 activated black ash sample. Locations and proportions of corresponding peaks are shown in Table 7. When compared with the original black ash the intensities of belite/alite and quartz peaks are lowered. The new peaks at –79,15; –82,29; –85,5 and –92,45 ppm were assigned to Q1; Q2; Q2 and C–S–H gel, respectively. The broad C–S–H gel peak is similar to sodium disilicate activated sample in which the aluminosilicate chains are longer than in Portland cement because the center of the peak at –92,45 ppm indicates to Q3 branching silicate sites.

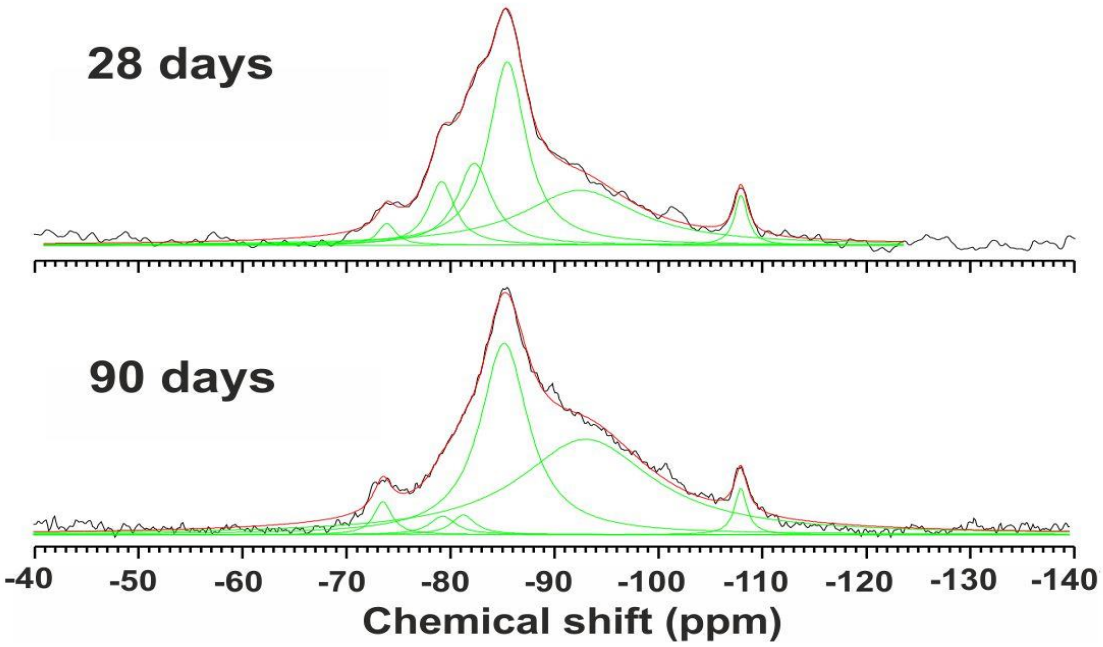


**Figure 14.** $^{29}$Si MAS-NMR spectra of sodium disilicate with $SiO_2/Na_2O$ 1,5 activated black ash after 28 and 90 days.

**Table 7.** Locations and proportions of peaks in $^{29}$Si MAS-NMR spectrum of sodium disilicate with $SiO_2/Na_2O$ 1,5 activated black ash and original black ash.

| | Belite/Alite | Q1 | Q1 | Q2 | Q2 | Glass | CSH | Glass | Quartz |
|---|---|---|---|---|---|---|---|---|---|
| Days/ppm | -73,5 | -79,15 | -81,23 | -82,29 | -85,5 | -89,1 | -92,45 | -98,3 | -108 |
| Bash | 0,29 | | | | | 0,41 | | 0,24 | 0,06 |
| C28 | 0,02 | 0,09 | | 0,15 | 0,37 | | 0,34 | | 0,03 |
| C90 | 0,02 | 0,02 | 0,02 | | 0,38 | | 0,53 | | 0,02 |

After 90 days the intensity of the C–S–H peak has risen, indicating that the amount of C–S–H gel in sample hasincreased. The increase can be attributed to the incorporation of Q2 silicon chain midmember species into the amorphous structure. The mean chain length of the silicate structure accompaning the C–S–H phase increases from 13,6 at 28 days to 22 at 90 day. These changes show an ongoing polycondensation reaction from 28 to 90 days.

For an easier overview and comparison of the $^{29}$Si MAS-NMR results, the positions and corresponding silicate structures of all the samples are collectively given in Appendix C.

## 5.3. Strength Development

When comparing the structural changes and compressive strength of the samples (Appendix D) it was observed that water activated sample presents strength development to high values, which may be associated with microstructure and secondary mineralisation (Paaver 2014).

Sample activated with NaOH show low initial compressive strength and further growth in strength correlates well with the dissolution and development of the silicate structures in NaOH activated samples.

The initial strength in sodium disilicate based samples correlates well with the geopolymeric structure of the silicate phases. Altough the $^{29}$Si MAS-NMR and ATR-FTIR show that the polycondensation is ongoing and the structure is strengthening, the observed lower compressive strength values of the samples can be attributed to shrinkage of the material and changes in microstructure (Paaver 2014)

# 6. CONCLUSIONS

In the current thesis, three different activator solutions alongside water were used to synthesise geopolymeric binders from black ash. It was proven that some extent of geopolymerisation takes place in every sample of activated black ash, indicating that black ash could be used to produce geopolymeric materials. Producing cement from geopolymers instead of Portland cement would be 60% energy-efficient and emit up to 80% less carbon dioxide. Producing cements from black ash would be a sustainable utilization for otherwise useless hazardous waste.

In sodium disilicate ($SiO_2/Na_2O$ 2,72) activated sample calcium silicate hydrate gel is formed, which is the phase connected to the strength of Portland cement. The $^{29}Si$ MAS-NMR and ATR-FTIR spectra indicate that the gel contains polymeric parts in which the polymer is mainly formed of silicate middle groups (Q2) and the silicate chains are lengthening in time. These factors are responsible for the strength and further strengthening of the material. The samples of black ash activated with sodium disilicate $SiO_2/Na_2O$ 1,5 show similar characteristics. However the NMR spectrum reveals that the amorphous geopolymeric phase (C–S–H gel) is accompanied by a two dimensional silicate chain structure which is also characteristic of C–S–H phase.

In NaOH activated black ash samples, it was observed that it contains silicate structures with short chain lengths and also a content of undissolved amorphous phase from the source material. This indicates that NaOH solution was not sufficient in dissolving the amorphus phase present in source material and the depolymerized silicate species have not substantially polycondensed.

Based on the results of this thesis the synthesis of geopolymeric products from black ash can be achieved with activator solutions containing soluble silica. Altough further research is needed to establish the optimal ratios of activator solutions the results show a proof of concept.

## ACKNOWLEDGEMENTS

I would like to thank Ivo Heinmaa from National Institute of Chemical Physics and Biophysics for the NMR analyses and Signe Vahur for assistance in studying the ATR-FTIR method. I would also like to thank Peeter Paaver for all the help.

## REFERENCES


ASTM C618, 2008. Standard Specification for Coal Fly Ash and Raw or Calcined Natural Pozzolan for Use in Concrete. ASTM International.

Davidovits, J., 1988. Geopolymer chemistry and properties. In: Davidovits, J., Orlinski, J. (Eds.), Proceedings of the 1st International Conference on Geopolymer '88, vol. 1, Compiegne, France, 1–3 June, 25–48.

Davidovits, J., 1991. Geopolymers: Inorganic polymeric new materials. Journal of Thermal Analysis 37, 1633–1656.

Davidovits, J., 2011. Geopolymer Chemistry and Applications, 3rd Edition. Institut Géopolymére, France.

Davidovits, J., 2013. A review on Geopolymer cement, as of January 2013. Institut Géopolymére, France.

Duxson, P., Fernandez-Jimenez, A., Provis, J.L., Lukey, G.C., Palomo, A. & van Deventer, J.S.J., 2007. Geopolymer technology: the current state of the art. Journal of Materials Science 42(9), 2917–2933.

Fernández-Carrasco, L., Torrens-Martín, D., Morales, L.M., Martínez-Ramírez, S., 2012. Infrared Spectroscopy in the Analysis of Building and Construction Materials, Infrared Spectroscopy – Materials Science, Engineering and Technology, Prof. Theophanides Theophile (Ed.). ISBN: 978-953-51-0537-4, InTech.

García-Lodeiro, I., Fernandez-Jimenez, A., Blanco-Varela, M.T., Palomo, A., 2007. Synthesis and characterization of cementitious gels (C–S–H and N–A–S–H). Compability studies. Eduardo Torroja Institute

García-Lodeiro, I., Macphee, D.E., Palomo, A., Fernández-Jiménez, A., 2009. Effect of alkalis on fresh C–S–H gels. FTIR analysis. Cement and Concrete Research 39, 147–153.

Guo, X., Shi, H. & Dick, W.A., 2010. Compressive strength and microstructural characteristics of class C fly ash geopolymer. Cement & Concrete Composites 32(2), 142–147.

Hornak, J.P., 1996. The Basics of NMR. [http://www.cis.rit.edu/htbooks/nmr/inside.htm] 17.05.2014

Komarneni, S., Roy, D.M., 1985. New tobermorite cation exchangers. Journal of Materials Science 20, 2930–2936.

Komnitsas, K., Zaharaki, D., 2007. Geopolymerisation: A review and prospects for the minerals industry. Minerals Engineering 20, 1261–1277.

Lecomte, I., Henrist, C., Liegeois, M., Maseri, F., Rulmont, A., Cloots, R., 2006. (Micro)-structural comparison between geopolymers, alkali-activated slag cement and Portland cement. Journal of the European Ceramic Society 26, 3789–3797.

Lee, W.K.W., van Deventer, J.S.J., 2003. Use of Infrared Spectroscopy to Study Geopolymerization of Heterogeneous Amorphous Aluminosilicates. Langmuir 19, 8726–8734.

Leito, I. 2013. NMR ja ESR spektroskoopia, teoreetiline sissejuhatus. [http://tera.chem.ut.ee/~ivo/ak2/NMR.pdf] 25.10.2013

Li, Q., Hu, X., Li, B., Li, F., Li, P., Shen, L. & Zhai, J., 2012. Synthesis of geopolymer composites from blends of CFBC fly and bottom ashes. Fuel 97, 366– 372.

Lippmaa, E., Mägi, M., Samoson, A., Engelhardt, G., Grimmer, A-R., 1980. Structural studies of silicates by solid state high resolution $^{29}$Si NMR. Journal of the American Chemical Society 102, 4889–4893.

Mägi, M., Lippmaa, E., Samoson, A., Engelhardt, G., Grimmer, A-R., 1984. Solid state high-resolution silicon-29 chemical shifts in silicates. Journal of Physical Chemistry 88, 1518–1522.

Ots, A., 2006. Oil Shale Fuel Combustion Tallinna Raamatutrükikoda, Tallinn, Estonia.

Paaver, P., 2014. Geopolymerization of the Estonian oil shale solid heat carrier retorting waste ash: changes in mineral-chemical composition and uniaxial compressive strength development. Bachelor of Science thesis. University of Tartu.

Rees, C.A., 2007. Mechanisms and kinetics of gel formation in geopolymers. Doctor of Philosophy thesis. University of Melbourne.

Reinik, J., Heinmaa, I., Mikkola, J.P., Kirso, U., 2007. Hydrothermal alkaline treatment of oil shale ash for synthesis of tobermorites. Fuel 86, 669–676.

Richardson, I.G., Groves, G.W., 1997. The structure of the calcium silicate hydrate phases present in hardened pastes of white Portland cement/blast-furnace slag blends.
Journal of Materials Science 32, 4793–4802

Roy, A., Schilling, P.J. & Eaton, H.C., 1996. Alkali Activated Class C Fly Ash Cement – Patent 5565028

Sedman, A., 2013. Strength and self-cementing properties of oil shale retorting wastes. Doctor of Philosophy thesis. University of Tartu.

Subaer, Van Riessen, A. 2007. Thermo-mechanical and microstructuraln characterisation of sodium-poly (sialate-siloxo) (Na-PSS) geopolymers. Journal of Materials Science 42 (9): 3117–3123.

Teearu, A., 2009. Investigation of pigments with ATR-FTIR spectroscopy. Master of Science thesis. University of Tartu.

Teedumäe, A., Raukas, A., 2006. The possibility of integrating sustainability into legal framework for use of oil shale reserves. Oil Shale 23 (2) 119–124

Van Deventer, J.S.J., Provis, J.L., Duxson, P., Lukey, G.C., 2007. Reaction mechanisms in the geopolymeric conversion of inorganicwaste to useful products. Journal of Hazardous Materials 139 (3), 506–513.

Viru Keemia Grupp homepage [http://www.vkg.ee/est/arendustegevus/kasutatavad-tehnoloogiad/petroter] 17.05.2014

Xu, H., Van Deventer, J.S.J., 2000. The geopolymerisation of aluminosilicate minerals. International Journal of Mineral Processing 59 (3), 247–266.

Yip, C.K., Lukey, G.C., Van Deventer, J.S.J., 2005. The coexistence of geopolymeric gel and calcium silicate hydrate at the early stage of alkaline activation. Cement and Concrete Research 35 (9), 1688–1697.

## APPENDIXES

**Appendix A.** Mineralogical compositions of black ash and samples.

| Phase/Sample | BAsh | A7 | A28 | A90 | C7 | C28 | C90 | B7 | B28 | B90 | E7 | E28 | E90 |
|---|---|---|---|---|---|---|---|---|---|---|---|---|---|
| **Quartz** | 11,71 | 7,39 | 6,67 | 7,85 | 8,68 | 13,32 | 7,75 | 10,08 | 13,30 | 8,39 | 11,68 | 11,91 | 10,72 |
| **Orthoclase** | 14,25 | 11,83 | 10,39 | 12,14 | 11,16 | 13,70 | 10,47 | 11,99 | 11,52 | 10,03 | 12,54 | 11,28 | 12,34 |
| **Muscovite** | 2,64 | 6,91 | 7,10 | 7,21 | 5,88 | 8,33 | 7,15 |  | 1,45 | 5,05 | 1,74 | 3,44 | 5,65 |
| **Calcite** | 26,81 | 18,85 | 16,48 | 19,20 | 19,56 | 27,17 | 20,99 | 23,64 | 25,77 | 21,71 | 23,23 | 28,42 | 25,58 |
| **Vaterite** |  | 1,48 | 1,90 | 2,11 | 1,37 | 1,62 | 1,47 | 2,40 | 2,75 | 2,92 | 2,88 | 0,21 | 1,46 |
| **Dolomite** | 8,52 | 5,73 | 5,47 | 4,97 | 5,69 | 4,85 | 5,88 | 6,57 | 7,12 | 4,70 | 8,55 | 11,83 | 6,04 |
| **Lime** | 2,08 |  |  |  |  |  |  |  |  |  |  |  |  |
| **Portlandite** |  |  |  |  |  |  |  | 1,51 | 2,14 | 0,68 | 1,21 | 0,28 | 0,44 |
| **Periclase** | 7,50 | 3,16 | 2,15 | 2,06 | 3,77 | 4,15 | 2,51 | 2,49 | 2,67 | 2,15 | 2,19 | 1,90 | 1,89 |
| **C2S β** | 3,15 | 2,33 | 2,38 | 2,53 | 2,67 | 2,77 | 2,34 | 5,77 | 6,88 | 6,85 | 5,75 | 6,67 | 7,11 |
| **Merwinite** | 5,22 | 1,99 | 2,32 | 1,47 | 2,57 | 3,59 | 2,14 | 2,77 | 2,82 | 2,45 | 2,18 | 1,61 | 1,34 |
| **Melilite** | 4,19 | 2,56 | 3,33 | 2,65 | 2,84 | 2,89 | 3,02 | 3,79 | 3,04 | 2,13 | 2,05 | 2,60 | 2,89 |
| **Wollastonite** | 1,53 | 3,67 | 4,33 | 4,20 | 3,96 | 5,95 | 4,90 | 3,79 | 3,40 | 3,15 | 2,50 | 3,08 | 4,29 |
| **Oldhamite** | 3,59 | 1,70 | 0,84 | 0,76 | 1,98 | 1,31 | 0,75 | 0,67 | 0,56 | 0,39 | 0,00 | 0,00 | 0,03 |
| **Anhydrite** | 1,10 |  |  |  |  |  |  |  |  |  |  |  |  |
| **Gypsum** |  |  |  |  |  |  |  | 0,95 | 1,32 | 2,33 | 0,93 | 0,66 | 0,95 |
| **Hydrocalumite** |  |  |  |  |  |  |  | 17,93 | 13,30 | 16,55 | 13,90 | 5,97 | 11,08 |
| **Ettringite** |  |  |  |  |  |  |  | 0,01 |  |  | 4,71 | 7,59 | 6,33 |
| **Montmorillonite** |  |  |  |  |  |  |  | 0,49 | 0,02 | 2,09 |  |  |  |
| **Hematite** | 1,09 | 0,71 | 0,33 | 0,79 | 0,78 | 0,97 | 0,64 | 0,43 | 0,18 | 0,13 | 0,47 | 0,36 | 0,60 |
| **Magnetite** | 0,94 | 0,69 | 0,92 | 0,61 | 0,90 | 1,26 | 0,94 | 1,07 | 1,58 | 1,19 | 1,30 | 1,80 | 1,18 |
| **Amorphus** | 5,70 | 30,98 | 35,40 | 31,47 | 28,22 | 8,14 | 29,07 | 3,67 | 0,20 | 7,13 | 2,18 | 0,41 | 0,07 |

**Appendix B.** $^{29}$Si MAS-NMR proportions of the peaks in different samples.

| **BA + sodium disilicate** | | | | | | |
|---|---|---|---|---|---|---|
| | **BlackAsh** | | **A28** | | **A90** | |
| Site | ppm | % | ppm | % | ppm | % |
| Belite/Alite | -72,69 | 0,29 | - | - | - | - |
| CSH (Q2) | - | - | -88,7 | 0,94 | -90,6 | 0,9 |
| Glass | -89,1 | 0,41 | - | - | - | - |
| Glass | -98,3 | 0,24 | - | - | - | - |
| Q4 | - | - | -108,7 | 0,05 | -106,6 | 0,09 |
| Quartz | -108,11 | 0,06 | -108,4 | 0,01 | -107,8 | 0,01 |

| **BA + NaOH** | | | | | | |
|---|---|---|---|---|---|---|
| | **BlackAsh** | | **B28** | | **B90** | |
| Site | ppm | % | ppm | % | ppm | % |
| Belite/Alite | -72,69 | 0,29 | -73,13 | 0,03 | -73,25 | 0,04 |
| Q1 | - | - | -78,92 | 0,28 | -79 | 0,22 |
| Q2(1Al) | - | - | -81,74 | 0,19 | -80,76 | 0,16 |
| Q2 | - | - | -84,01 | 0,17 | -84,7 | 0,29 |
| Glass | -89,1 | 0,41 | - | - | - | - |
| Q3 | - | - | -96,5 | 0,27 | -97,3 | 0,26 |
| Glass | -98,3 | 0,24 | - | - | - | - |
| Q3 | - | - | -100,8 | 0,01 | - | - |
| Quartz | -108,11 | 0,06 | -108,02 | 0,05 | -107,9 | 0,02 |

| BA + NaOH + sodium disilicate | | | | | | |
|---|---|---|---|---|---|---|
| | **BlackAsh** | | **C28** | | **C90** | |
| Site | ppm | % | ppm | % | ppm | % |
| Belite/Alite | -72,69 | 0,29 | -73,87 | 0,02 | -73,5 | 0,02 |
| Q1 | - | - | -79,15 | 0,09 | -79,25 | 0,02 |
| Q1 | - | - | - | - | -81,23 | 0,02 |
| Q2 | - | - | -82,29 | 0,15 | - | - |
| Q2 | - | - | -85,5 | 0,37 | -85,16 | 0,38 |
| Glass | -89,1 | 0,41 | - | - | - | - |
| CSH | - | - | -92,45 | 0,34 | -93,02 | 0,53 |
| Glass | -98,3 | 0,24 | - | - | - | - |
| Quartz | -108,11 | 0,06 | -107,9 | 0,03 | -107,9 | 0,02 |

| BA + $H_2O$ | | | | | | |
|---|---|---|---|---|---|---|
| | **BlackAsh** | | **E28** | | **E90** | |
| Site | ppm | % | ppm | % | ppm | % |
| Belite/Alite | -72,69 | 0,29 | -73,21 | 0,07 | -73,13 | 0,06 |
| Q1 | - | - | -79,89 | 0,19 | -82,54 | 0,15 |
| Q2 | - | - | -85,2 | 0,38 | - | - |
| Q2 | - | - | - | - | -86,16 | 0,08 |
| Glass | -89,1 | 0,41 | - | - | - | - |
| Glass | - | - | - | - | -91,63 | 0,65 |
| CSH | - | - | -95,4 | 0,19 | - | - |
| CSH | - | - | -95,42 | 0,01 | - | - |
| Glass | -98,3 | 0,24 | - | - | - | - |
| Q3 | - | - | -100,95 | 0,06 | - | - |
| Quartz | -108,11 | 0,06 | -108,1 | 0,11 | -108,2 | 0,06 |

**Appendix C.** Peak positions, proportions and corresponding silicate structures in 29Si MAS-NMR spectra.

| | **Belite/Alite** | **Q1** | **Q2(1Al)** | **Q2** | **Q2** | **Q2** | **CSH** | **Amorph** | **CSH** | **Amorp** | **CSH** | **CSH** | **Q3** | **Amorph** | **Q3** | **Q4** | **Q4** | **Quartz** |
|---|---|---|---|---|---|---|---|---|---|---|---|---|---|---|---|---|---|---|
| **ppm** | **-73,13** | **-78,92** | **-81,74** | **-82,29** | **-84,01** | **-86,16** | **-88,7** | **-89,1** | **-90,6** | **-91,63** | **-92,45** | **-95,4** | **-96,5** | **-98,3** | **-100,9** | **-106,6** | **-108,7** | **-108,1** |
| **Bash** | 0,29 | | | | | | | 0,41 | | | | | | 0,24 | | | | 0,06 |
| **A28** | | | | | | | 0,94 | | | | | | | | | | 0,05 | 0,01 |
| **A90** | | | | | | | | | 0,9 | | | | | | | 0,09 | | 0,01 |
| **B28** | 0,03 | 0,28 | 0,19 | | 0,17 | | | | | | | | 0,27 | | 0,01 | | | 0,05 |
| **B90** | 0,04 | 0,22 | 0,16 | | 0,29 | | | | | | | | 0,26 | | | | | 0,02 |
| **C28** | 0,02 | 0,09 | | 0,15 | 0,37 | | | | | | 0,34 | | | | | | | 0,03 |
| **C90** | 0,02 | 0,02 | 0,02 | | 0,38 | | | | | | 0,53 | | | | | | | 0,02 |
| **E28** | 0,07 | 0,19 | | | 0,38 | | | | | | | 0,20 | | | 0,06 | | | 0,11 |
| **E90** | 0,06 | 0,15 | | | | 0,08 | | | | 0,65 | | | | | | | | 0,06 |

**Appendix D.** Compressive strengths of the samples (Paaver 2014).

| | **BA+sodiumdisilicate** | | | **BA+NaOH** | | | **BA+sodiumdisilicate** | | | **BA+water** | | |
|---|---|---|---|---|---|---|---|---|---|---|---|---|
| **Days** | 7 | 28 | 90 | 7 | 28 | 90 | 7 | 28 | 90 | 7 | 28 | 90 |
| **Compressive strength (Mpa)** | 10,4 | 4,9 | 6,3 | 1,2 | 1,5 | 4,5 | 7,8 | 6,7 | 5,2 | 2,2 | 7,2 | 9,8 |

# KOKKUVÕTE

## Põlevkiviõlitööstuse jääktuha geopolümeriseerumine: struktuursete muutuste kirjeldamine infrapuna- (ATR-FTIR) ja tuumamagnetresonantsspektroskoopia ($^{29}$Si MAS-NMR) meetodite abil

Marian Külaviir

Seoses nafta maailmaturu hindade tõusuga suureneb nõudlus põlevkiviõli toodete järgi ning põlevkivi kasutamine soojuselektrijaamades väheneb järk-järgult. Seetõttu tekib lähitulevikus üha enam põlevkiviõli tootmise jääke, millele pole veel taaskasutust leitud ning praegu kasutatav tuha prügilatesse ladustamine on väga keskkonnaohtlik. Põlevkiviõli tööstuses kasutatakse tahke soojuskandja utmistehnoloogiat, millest pärast õlitootmisprotsessi jääb järele tuhk, mida oma värvuse tõttu kutsutakse ka mustaks tuhaks. Must tuhk on oma koostiselt sarnane kõrge kaltsiumisisaldusega C klassi (ASTM 2008) lendtuhaga. Klass C lendtuhast on varasemate uuringute põhjal (Guo *et al.* 2010) sünteesitud geopolümeerseid tsemente, mis loob head eeldused musta tuha kasutamiseks geopolümeeride toorainena.

Geopolümeerid on alumosilikaatsed anorgaanilised polümeerid millel on potentsiaal asendada praegu kasutusel olevaid tsemente, plastikuid ja muid mineraalidel põhinevaid tooteid. Võrreldes konventsionaalse Portland tsemendiga oleks geopolümeeridest tsemendi tootmine 60% energiasäästlikum ja emiteeriks 80% vähem süsinikdioksiidi (Li *et al.* 2012).

Käesolevas bakalaureusetöös uuriti mustast tuhast sünteesitud tsemetsete materjalide struktuure, eeldusel, et tuhaproovidesse on tekkinud geopolümeersed alumosilikaatsed struktuurid. Tsementatsiooni esilekutsumiseks aktiveeriti must tuhk vee, naatriumhüdroksiidi ja naatriumdisilikaadi lahusega. Proovide struktuuri analüüsiks kasutati ATR-FTIR ja $^{29}$Si MAS-NMR spektroskoopiat.

Spektrite tõlgendamisel leiti, et kõikides proovides leiab aset silikaatse aine polümeriseerumine, kinnitades seda, et mustast tuhast on võimalik toota geopolümeerseid materjale. Võrreldes spektreid ja vastavaid survetugevusi, leiti, et mustast tuhast geopolümeeride tootmiseks on kõige optimaalsem kasutada lahustunud ränidioksiidi sisaldavat aktivaatorlahust.

**Non-exclusive licence to reproduce thesis and make thesis public**

I, ____Marian Külaviir_____,
(*author's name*)

1. herewith grant the University of Tartu a free permit (non-exclusive licence) to:

1.1. reproduce, for the purpose of preservation and making available to the public, including for addition to the DSpace digital archives until expiry of the term of validity of the copyright, and

1.2. make available to the public via the web environment of the University of Tartu, including via the DSpace digital archives until expiry of the term of validity of the copyright,

___ Geopolymerization of the Estonian oil shale solid heat carrier retorting waste ash: characterization of structural changes through infrared (ATR-FTIR) and nuclear magnetic resonance spectroscopic (29Si MAS-NMR) analysis_____,
(*title of thesis*)

supervised by _____Päärn Paiste and Martin Liira_____,
(*supervisor's name*)

2. I am aware of the fact that the author retains these rights.

3. I certify that granting the non-exclusive licence does not infringe the intellectual property rights or rights arising from the Personal Data Protection Act.

Tartu 23.05.2014